

Traffic Jams Reduce Hydrolytic Efficiency of Cellulase on Cellulose Surface

| | |
|-------|---|
| メタデータ | 言語: eng 出版者: 公開日: 2017-10-03 キーワード (Ja): キーワード (En): 作成者: メールアドレス: 所属: |
| URL | https://doi.org/10.24517/00010416 |

This work is licensed under a Creative Commons Attribution-NonCommercial-ShareAlike 3.0 International License.



Traffic Jams Reduce Hydrolytic Efficiency of Cellulase on Cellulose Surface

Kiyohiko Igarashi^{1*†}, Takayuki Uchihashi^{2-4*}, Anu Koivula⁵, Masahisa Wada^{1, 6}, Satoshi Kimura^{1, 6}, Tetsuaki Okamoto^{1, 2}, Merja Penttilä⁵, Toshio Ando²⁻⁴, and Masahiro Samejima¹

¹ Department of Biomaterial Sciences, Graduate School of Agricultural and Life Sciences, The University of Tokyo, Bunkyo-ku, Tokyo 113-8657, Japan

² Department of Physics, Kanazawa University, Kanazawa 920-1192, Japan,

³ Bio-AFM Frontier Research Center, College of Science and Engineering, Kanazawa University, Kakuma-machi, Kanazawa 920-1192, Japan

⁴ Core Research for Evolutional Science and Technology, Japan Science and Technology Agency, Sanbon-cho, Chiyoda-ku, Tokyo 102-0075, Japan

⁵ VTT Technical Research Centre of Finland, P.O. Box 1000, FI-02044 VTT, Finland

⁶ Department of Plant and Environmental New Resources, College of Life Sciences, Kyung Hee University, 1, Seocheon-dong, Giheung-ku, Yongin-si, Gyeonggi-do 446-701, Republic of Korea

*These authors contributed equally to this work.

†To whom correspondence should be addressed. E-mail: aquarius@mail.ecc.u-tokyo.ac.jp

Abstract

A deeper mechanistic understanding of the saccharification of cellulosic biomass could enhance the efficiency of biofuels development. We report here the real-time visualization of crystalline cellulose degradation by individual cellulase enzymes using an advanced version of high-speed atomic force microscopy. *Trichoderma reesei*

cellobiohydrolase I (*TrCel7A*) molecules were observed to slide unidirectionally along the crystalline cellulose surface, but at one point exhibited collective halting analogous to a traffic jam. Changing the crystalline polymorphic form of cellulose by an ammonia treatment increased the apparent number of accessible lanes on the crystalline surface and consequently the number of moving cellulase molecules. Treatment of this bulky crystalline cellulose simultaneously or separately with *T. reesei* cellobiohydrolase II (*TrCel6A*) resulted in a significant increase in the proportion of mobile enzyme molecules on the surface. Cellulose was completely degraded by the synergistic action between the two enzymes.

Biorefining encompasses production of fuels, power, heat, and value-added chemicals appropriate conversion of lignocellulosic feedstocks. This prospect offers many advantages, including diminished carbon dioxide emission, productive use of renewable non-food crops or inedible waste products, and reduction of petroleum use. One of the bottlenecks to widespread biorefining application is the enzymatic hydrolysis of the cellulosic raw material into sugars. In attempts to maximize efficiency and reduce costs, many studies on both individual cellulases and enzyme cocktails have been carried out (1). Various pre-treatment methods have also been examined to increase the amount of sugar generated from cellulosic biomass with reduced enzyme loading and energy consumption, aiming at the development of commercially viable bio-processes. It is generally recognized that one of the problems in cellulose hydrolysis is the slowdown of enzyme action with time and conversion (2, 3). Cellulose is a major component of plant cell walls, accounting for almost half of their net weight. Cell wall cellulose typically has about 70% crystallinity, suggesting that approximately one-third of net cellulosic biomass consists of natural crystalline cellulose, which is generally called cellulose I (4). Because cellulose chains have stable β -1,4-glucosidic

bonds and each chain is also stabilized by intra- and inter-molecular hydrogen bonds, cellulose I is quite resistant not only to chemical hydrolysis, but also to enzymatic degradation (5).

The industrially important cellulolytic ascomycete fungus *Trichoderma reesei* (anamorph of *Hypocrea jecorina*) secretes two extracellular cellobiohydrolases (CBHs), which are cellulases that can hydrolyze glycosidic linkages particularly at a crystalline surface, and form cellobiose (β -1,4-glucosidic dimer) as a major product from cellulose I (6). The two *T. reesei* CBHs hydrolyze crystalline cellulose from the reducing- and the non-reducing-ends, respectively (7). These enzymes have a similar two-domain organization: the cellulose-binding domain (CBD), which is categorized into carbohydrate-binding module (CBM) family 1, contributes to adsorption on the insoluble substrate, and the cellulose-hydrolyzing catalytic domain (CD) catalyzes cleavage of glycosidic bonds. The two *T. reesei* cellobiohydrolase CDs have different types of folds. The CD of CBH I belongs to the glycoside hydrolase (GH) family 7 and the CD of CBH II belongs to the GH family 6, as listed on the Carbohydrate-Active enZyme (CAZy) server (8), and thus the two enzymes are called *TrCel7A* and *TrCel6A*, respectively. In both cellobiohydrolases, the catalytic amino acids are located in a relatively long tunnel formed by surface loops extending from the central fold of the CD (9, 10). We previously visualized the linear movement of wild-type and isolated CD on cellulose I _{α} using high-speed atomic force microscopy (HS-AFM); the data suggested that the sliding movement of wild-type *TrCel7A* reflects the processive degradation of the cellulose chain by catalysis at the CD and requires initial recognition of the cellulose chain. The chain recognition involves the tryptophan residue W40 at the entrance of the *TrCel7A* active site tunnel (11).

In the present study, we succeeded in enhancing the temporal and spatial resolutions by using a laboratory-built HS-AFM with extensive improvements over the version reported

previously (12), and we were able to visualize the movement of *TrCel7A* molecules on crystalline cellulose in detail. Figure 1A and movie S1 show enzyme molecules sliding unidirectionally on the cellulose I_{α} surface. This movement of *TrCel7A* was observed only at the top of the cellulose crystal, where the individual enzyme molecules were moving as one line. The movement of the *TrCel7A* molecules was analyzed by employing a custom software to track the linear movement of the center of each molecule, and the time course of molecular movement is shown in Figure 1B. Some molecules slid continuously without stopping (demonstrated *e.g.* by the orange plot in Fig. 1B) whereas the movement of other *TrCel7A* molecules was often disturbed by halted and/or more slowly moving molecules (demonstrated *e.g.* by the open green and closed red plots in Fig. 1B), resembling the movement of traffic on a road. According to the histogram of the measured velocities (Fig. 1C), there would seem to be two populations of *TrCel7A* molecules having average velocities of -0.32 ± 3.4 and 7.1 ± 3.9 nm/s. This is consistent with the idea that *TrCel7A* molecules intermittently repeat stop and go movements. It is generally believed that CBHs have two modes of adsorption on a cellulose surface: the productive adsorption mode in which both the CD and CBD contribute to the binding, and the non-productive adsorption mode in which the enzyme molecules bind only via the CBD (13). In our previous HS-AFM study with *TrCel7A* and its mutants, that variant that bound only via the CBD (*i.e.* W40A without tryptophan residue at the active-site entrance) did not remain long on the surface and therefore could not be continuously visualized (11). In contrast, molecules bound to the substrate chain via the CD (*i.e.* the *TrCel7A* wild-type enzyme, isolated CD without CBD, and the inactive mutant E212Q) could be continuously visualized during HS-AFM observation. Considering these results, it seems likely that the *TrCel7A* molecules visualized here as stationary in the middle of cellulose fibrils have been stopped while holding a substrate chain in the active site tunnel of the CD. Moreover, we previously reported an average velocity of 3.5 ± 1.1 nm/s for the

movement of *TrCel7A* (*II*), as shown by a dotted line in Fig. 1B. The velocity of moving molecules obtained in the present study was 7.1 ± 3.9 nm/s, *i.e.* twice the velocity estimated in the previous study, whereas the averaged velocity for all molecules (stopped and moving) was 5.3 ± 4.9 nm/s. Therefore, it seems likely that this earlier value (for average velocity) was determined by the two populations of moving and stopped molecules. Although the time-resolution of the HS-AFM observation used in this study was up to 300 ms/frame, more than 3 times faster than that in the previous work (up to 1 s/frame), this time-resolution is still not high enough to analyze each hydrolytic step of *TrCel7A*. If one hydrolytic cycle produces one cellobiose unit, which is approximately 1 nm in length, each individual hydrolysis-related movement could occur within 140 ms, as calculated from the velocity obtained in the present study.

As already mentioned, cellulose I is quite resistant to enzymatic hydrolysis. We have shown recently that crystalline polymorphic conversion from cellulose I to cellulose III_I by supercritical ammonia treatment dramatically enhances the hydrolysis of crystalline cellulose by *TrCel7A* (*14*). In order to investigate the reason for the enhanced hydrolysis of cellulose III_I, the degradation of the crystalline celluloses was visualized by HS-AFM and the results were compared with those of the conventional adsorption study. The binding isotherms, plots of free enzyme concentration versus amount of adsorbed enzyme ($[F]-A$), followed a Langmuir-type two-binding site model on both crystalline celluloses (cellulose I_α and III_I) (Fig. 2A). These data show that *TrCel7A* has higher binding capacity to cellulose III_I than to cellulose I_α. The simulated curves were divided into high-affinity (solid line) and low-affinity (dashed line) components, as shown in Fig. 2B. There was no significant difference in the low-affinity component between the two crystalline polymorphs, whereas the high-affinity component in the case of crystalline cellulose III_I was quite large compared with that of crystalline cellulose I_α consistent with our previous study (*14*).

When the hydrolysis of crystalline cellulose III_I by *TrCel7A* was observed by HS-AFM, as shown in Fig. 2C and movie S2, differences were apparent in the number but not in the velocity of enzyme molecules moving on cellulose III_I and cellulose I_α. In the case of crystalline cellulose I_α, enzyme molecules slid only along limited lanes (Fig. 1A and movie S1), whereas on cellulose III_I *TrCel7A* molecules moved over almost the whole surface. This may reflect the difference in the amount of high-affinity binding (Fig. 2, A and B). Lehtiö and coworkers reported recently that the isolated CBD of *TrCel7A* binds to the 110 surface of *Valonia* cellulose (cellulose I_α), and they suggested that *TrCel7A* degrades crystalline cellulose from this hydrophobic surface (15). The hypothesis was recently confirmed by means of AFM observation (16). The characteristics of cellulose I_α and III_I differ (17, 18) in that cellulose I_α bears hydrophobic 110 surfaces between hydrophilic 100 and 010 surfaces, whereas cellulose III_I has similarly hydrophobic $\bar{1}\bar{1}0$ and hydrophilic 010 surfaces, but moderately hydrophobic (and larger) 100 surfaces, as shown in Fig. 2D. Because we used hydrophobic highly oriented pyrolytic graphite as a grid in the experiments, the crystals are expected to be oriented with their hydrophobic surfaces in contact with the grid, and by symmetry on the opposite, top face as well. Therefore, it appears that *TrCel7A* moved not only on the hydrophobic $\bar{1}\bar{1}0$ surface, but also on the (somewhat less) hydrophobic 100 surface, of cellulose III_I. In contrast, 110 is the only surface sufficiently hydrophobic for the enzyme to attach to in the case of cellulose I_α. Increasing the number of suitable lanes for cellulase movement would be an effective way to enhance crystalline cellulose hydrolysis, as judged from the comparison between cellulose I_α and cellulose III_I. In the case of *TrCel7A* action, moreover, when the movement of one molecule was halted, many following molecules stacked behind it on the cellulose III_I surface, causing a traffic jam as shown in Fig. 3A and movie S3. In Fig. 3B and movies S4 and S5, however, it became clear that after several additional molecules had also become blocked, the enzyme molecules started to move again

on the surface and a cellulose bundle was peeled off from the crystalline cellulose. This behavior may reflect the presence of an obstruction on the surface of crystalline cellulose, which a single *TrCel7A* molecule is unable to climb over, and is therefore halted. However, as schematically represented in Fig. 3C, the accumulation of subsequent molecules behind the blocked molecule seems to lead to elimination of the obstacle(s). As a result, the blocked molecules re-start linear movement from the point where the first molecule had stopped.

In the process of crystalline cellulose hydrolysis by *T. reesei*, two major cellobiohydrolases, *TrCel7A* and *TrCel6A*, synergistically contribute as described above (7, 19). Here, we imaged the hydrolytic processes with crystalline cellulose III_I in the presence of both *TrCel6A* and *TrCel7A*. The crystals were first observed without enzyme (Fig. 4A, movie S6), then incubated *TrCel6A* for 495 seconds (Fig. 4, B and C, movies S7 and S8), and the same crystalline cellulose was again visualized after further addition of *TrCel7A* (Fig 4, D, E and F, movies S7 and S9). As shown in Fig. 4, A-C and movie S8, the appearance of the cellulose crystals did not significantly change during incubation with *TrCel6A*, although many enzyme molecules were observed on the surfaces. When *TrCel7A* was added, enzyme molecules were seen to start moving from many points on the surface of the substrate, and the crystals apparently became thinner after the passage of the enzyme molecules, as shown in Fig. 4, D-F and movie S9. This degradation of crystalline cellulose was dramatically faster than was the case with *TrCel7A* alone (compare movie S2). We also examined this synergetic action between the two enzymes biochemically. Cellobiose production from the reaction mixture containing both *TrCel6A* and *TrCel7A* (blue line in Fig. 4G) was greater than the sum (dotted line) of production by the individual enzymes separately (green and red lines for *TrCel6A* and *TrCel7A*, respectively), confirming the occurrence of synergistic hydrolysis of crystalline cellulose by these two enzymes, in agreement with previous findings. This has been called exo-exo synergy (20). These two enzymes both have active sites located in a

tunnel that passes through the whole CD. The active site tunnel of *TrCel6A* is formed by two surface loops and is about 20 Å long, whereas that of *TrCel7A* is approximately 50Å long, comprising six loops (9, 10, 21, 22). Previous transmission electron microscopic observations of crystalline cellulose after hydrolysis by *TrCel6A* and *TrCel7A* demonstrated that the two enzymes degrade the substrate from different ends of the crystal, *i.e.*, *TrCel7A* degrades the substrate from the reducing end, leading to fibrillation, thinning of the crystal or narrowing of the crystal end, whereas *TrCel6A* hydrolyzes the cellulose chain from the non-reducing end, less processively than *TrCel7A*, thereby sharpening the crystal tip (23, 24). It is somewhat difficult to find an explanation for this type of synergistic action on highly crystalline cellulose. One possibility is that the two loops forming the active site tunnel of *TrCel6A* can open and allow generation of nicks in the middle of crystalline cellulose and these nicks become starting and ending points for *TrCel7A* activity. This mode of synergistic action (schematically shown in Fig. 4H) could also be called endo-exo synergy (25), although, as explained above, *TrCel6A* is generally defined as an exo-glucanase (cellobiohydrolase). The synergistic hydrolysis was also observed when *TrCel7A* and *TrCel6A* were incubated at the same time with cellulose III_I.

The present results suggest that the roughness of the crystalline cellulose surface leads to the formation of traffic jams of productively bound cellulases. Thus, flattening the surface, removing obstacles and/or increasing the number of lanes, entrances, and exits by means of pretreatment or combined use of synergistically acting enzymes should reduce the molecular congestion, thereby improving the mobility of the cellulase molecules and increasing the efficiency of hydrolysis.

References and Notes

1. M. E. Himmel *et al.*, *Science* **315**, 804 (2007).

2. J. Jalak, P. Valjamae, *Biotechnol Bioeng* **106**, 871 (2010).
3. B. Yang, D. M. Willies, C. E. Wyman, *Biotechnol Bioeng* **94**, 1122 (2006).
4. D. N. S. Hon, *Cellulose* **1**, 1 (1994).
5. R. Wolfenden, Y. Yuan, *J. Am. Chem. Soc.* **130**, 7548 (2008).
6. T. T. Teeri, *Trends Biotechnol.* **15**, 160 (1997).
7. T. T. Teeri *et al.*, *Biochem. Soc. Trans.* **26**, 173 (1998).
8. B. Henrissat, A. Bairoch, *Biochem. J.* **293**, 781 (1993).
9. C. Divne *et al.*, *Science* **265**, 524 (1994).
10. J. Rouvinen, T. Bergfors, T. Teeri, J. K. Knowles, T. A. Jones, *Science* **249**, 380 (1990).
11. K. Igarashi *et al.*, *J. Biol. Chem.* **284**, 36186 (2009).
12. T. Ando *et al.*, *Proc. Natl. Acad. Sci. USA* **98**, 12468 (2001).
13. J. Ståhlberg, G. Johansson, G. Pettersson, *Bio/Technology* **9**, 286 (1991).
14. K. Igarashi, M. Wada, M. Samejima, *FEBS J.* **274**, 1785 (2007).
15. J. Lehtiö *et al.*, *Proc. Natl. Acad. Sci. USA* **100**, 484 (2003).
16. Y. S. Liu *et al.*, *J Biol Chem* **286**, 11195 (2011).
17. M. Wada, H. Chanzy, Y. Nishiyama, P. Langan, *Macromolecules* **37**, 8548 (2004).
18. Y. Nishiyama, J. Sugiyama, H. Chanzy, P. Langan, *J. Am. Chem. Soc.* **125**, 14300 (2003).
19. L. E. R. Berghem, L. G. Pettersson, U. B. Axiofredriksson, *Eur. J. Biochem.* **53**, 55 (1975).
20. B. Nidetzky, W. Steiner, M. Hayn, M. Claeysens, *Biochem J* **298**, 705 (1994).
21. C. Divne, J. Stahlberg, T. T. Teeri, T. A. Jones, *J Mol Biol* **275**, 309 (1998).
22. A. Koivula *et al.*, *J Am Chem Soc* **124**, 10015 (2002).

23. H. Chanzy, B. Henrissat, *FEBS Lett.* **184**, 285 (1985).
24. T. Imai, C. Boisset, M. Samejima, K. Igarashi, J. Sugiyama, *FEBS Lett.* **432**, 113 (1998).
25. T. M. Wood, S. I. McCrae, *Biochem. J.* **171**, 61 (1972).
26. K. Igarashi, M. Wada, R. Hori, M. Samejima, *FEBS J* **273**, 2869 (2006).
27. A. Koivula *et al.*, *Protein Expr Purif* **8**, 399 (1996).
28. H. Palonen, M. Tenkanen, M. Linder, *Appl Environ Microbiol* **65**, 5229 (1999)
29. M. Shibata, H. Yamashita, T. Uchihashi, H. Kandori, T. Ando, *Nature Nanotechnol* **5**, 208 (2010).
30. D. Yamamoto *et al.*, *Methods Enzymol* **475**, 541 (2010).
31. N. Kodera, D. Yamamoto, R. Ishikawa, T. Ando, *Nature*, **468**, 72 (2010).
32. K. Igarashi, M. Samejima, *Biosci Industry* **68**, 312 (2010).
33. K. Igarashi, T. Ishida, C. Hori, M. Samejima, *Appl Environ Microbiol* **74**, 5628 (2008).

Acknowledgements

The authors are grateful to Dr. Ken Tokuyasu in National Food Research Institute, Professor Jerry Ståhlberg in Swedish University of Agriculture Sciences, and Professor Akira Isogai in the University of Tokyo for their critical suggestions during the preparation of this paper. We thank Dr. Takeshi Tsukada for his help in checking the activity and purity of *TrCel6A*. This research was supported by Grants-in-Aid for Scientific Research to K.I. (no. 19688016 and 21688023), T.U. (no. 21023010 and 21681017), and to T.A. (no. 20221006) from the Japanese Ministry of Education, Culture, Sports, and Technology (MEXT), by a Grant for Development of Technology for High Efficiency Bioenergy Conversion Project to M.S. (no. 07003004-0) from the New Energy and Industrial Technology Development Organization (NEDO), and by a Grant for Development of Biomass Utilization Technologies for Revitalizing Rural Areas to M.S. from the Japanese Ministry of Agriculture, Forestry and Fisheries (MAFF).

Figure Legends

Fig. 1. (A) Real-time observation of crystalline cellulose I_{α} incubated with *TrCel7A* by means of HS-AFM. The time interval between images is 0.9 sec. These images are taken from movie S1. (B) Time course of distance from the initial position for *TrCel7A* molecules. The mobility of each molecule was analyzed using a routine developed in Igor Pro software, as described in Supporting Online Materials. The different symbols indicate different molecules observed in HS-AFM images. The black dotted line represents the average velocity of *TrCel7A* (3.5 nm/s) estimated by previous HS-AFM observation (11). (C) Velocity distribution of the linear movement of *TrCel7A* on crystalline cellulose I_{α} (n=188). The histogram was approximated by the combination

of two Gaussian distribution curves (blue line) with mean \pm SD values of -0.32 ± 3.4 (red) and 7.1 ± 3.9 (green).

Fig. 2. (A) Free *TrCel7A* concentration dependence of the amount of adsorbed enzyme on crystalline cellulose I_α (red) and III_I (blue). These plots were fitted to curves (red and blue solid lines) simulated by Langmuir's two-binding-site model as described in a previous report (26), and the high- (solid line) and low-affinity (dashed line) binding curves are individually drawn in (B). The binding parameters (A_1 , K_{ad1} , A_2 , K_{ad2}) of *TrCel7A* for cellulose I_α were 0.22 ± 0.02 , 8.4 ± 1.4 , 2.0 ± 0.2 , and 0.44 ± 0.09 , and those for cellulose III_I were 1.9 ± 0.1 , 11 ± 2 , 1.8 ± 0.3 , and 0.31 ± 0.06 (mean \pm SD), respectively. (C) HS-AFM images of crystalline cellulose III_I degradation by *TrCel7A*. The time interval between images is 30 sec. These images are taken from movie S2. (D) Schematic presentation of the increased number of observed lanes for *TrCel7A* on cellulose I_α (upper left) compared to cellulose III_I (upper right) and comparison of sections of crystalline cellulose I_α (bottom left) and cellulose III_I (bottom right) according to previous reports (17, 18).

Fig. 3. (A) Occurrence of molecular congestion of *TrCel7A* on cellulose III_I observed by means of HS-AFM. *TrCel7A* is moving from right to left. The time interval between images is 0.3 sec. These images are taken from movie S3. (B) Fibrillation of crystalline cellulose by *TrCel7A* after congestion was visualized by HS-AFM. The time interval between images is 1.5 sec. These images are taken from movie S5. (C) Schematic presentation of possible mechanism of fibrillation after the appearance of a traffic jam of *TrCel7A* molecules.

Fig. 4. Synergistic hydrolysis by *TrCel6A* and *TrCel7A* visualized by HS-AFM. (A) Microfibrils of cellulose III_I observed on the highly oriented pyrolytic graphite surface. B and C are images after 3.0 min (B) and 8.0 min (C) from the addition of 2.0 μM *TrCel6A*. D, E, and F are images after 0.5 min (D), 2.5 min (E) and 4.5 min (F) from the addition of *TrCel7A* following incubation with *TrCel6A* for 495 sec. A-C and D-F are acquired from movie S8 and S9, respectively. The numbers attached to the z-axes, which correspond to the maximum height in the lookup table (LUT), represent the maximum heights of the respective images. (G) Synergy between *TrCel6A* and *TrCel7A* in cellobiose production from cellulose III_I. Green and red plots are the rates of cellobiose production by *TrCel6A* and *TrCel7A*, respectively, and the blue plot shows the synergy between the two enzymes. The dotted line indicates the simple sum of cellobiose production calculated from the green and red plots. (H) Proposed mechanism for the exo-exo synergy between *TrCel6A* and *TrCel7A*.

Fig. 1

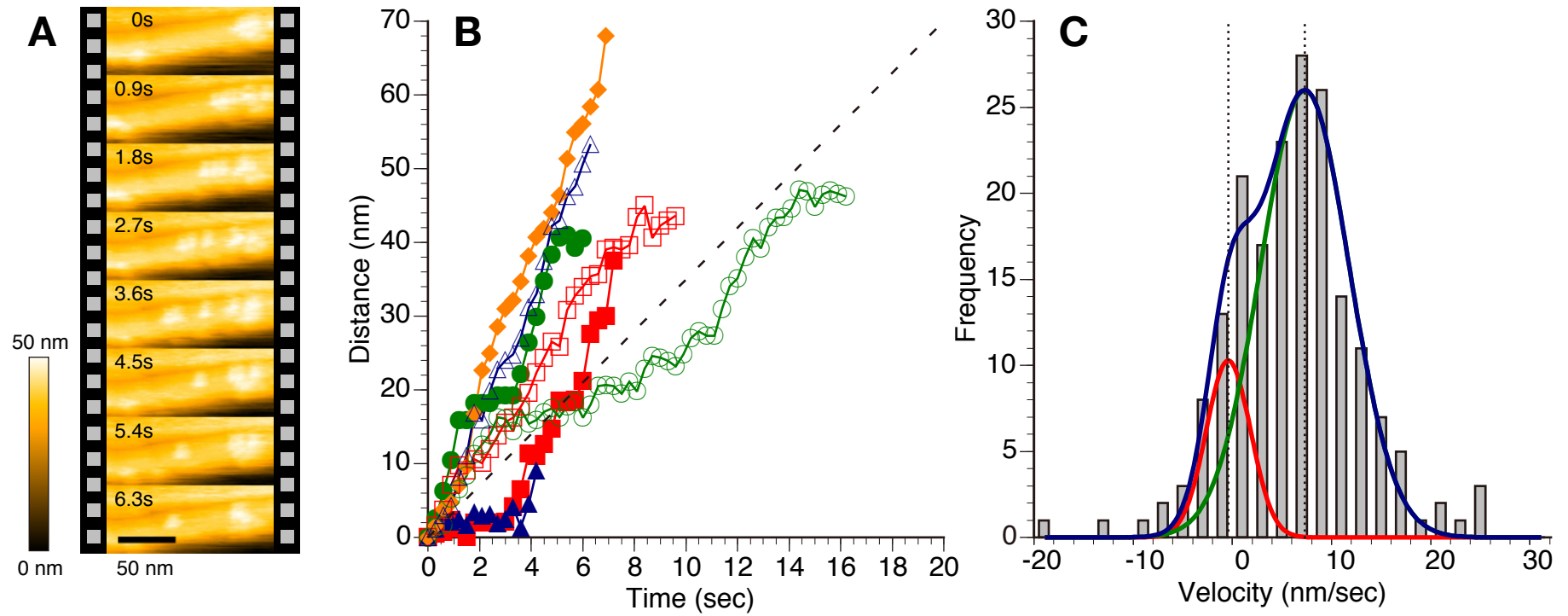


Fig. 2

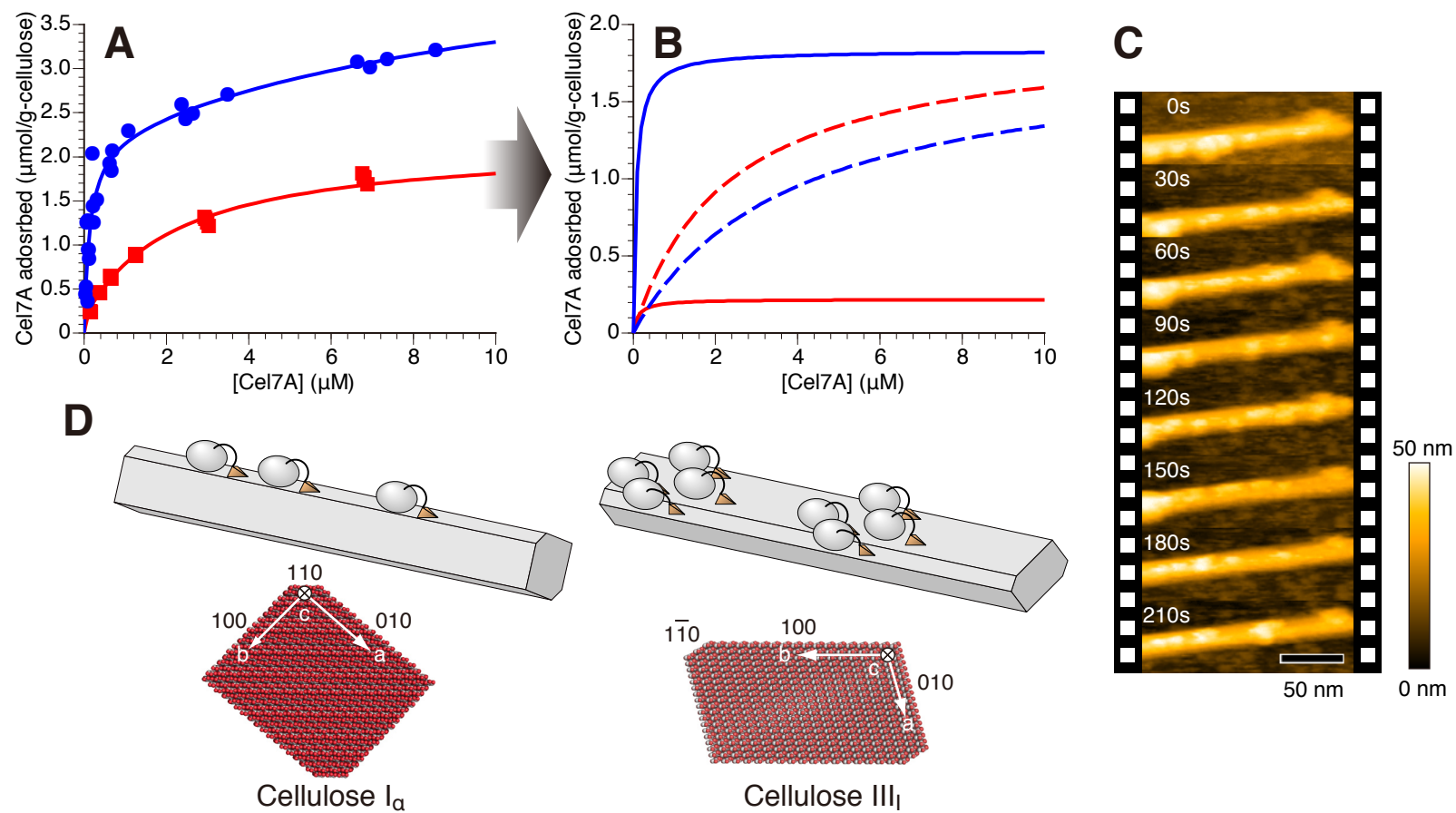


Fig. 3

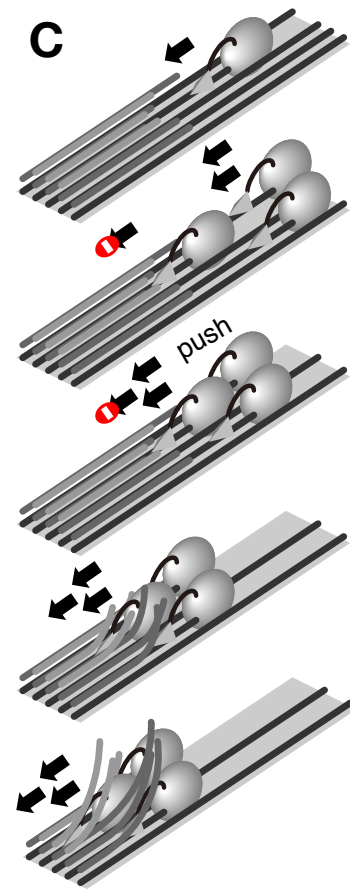
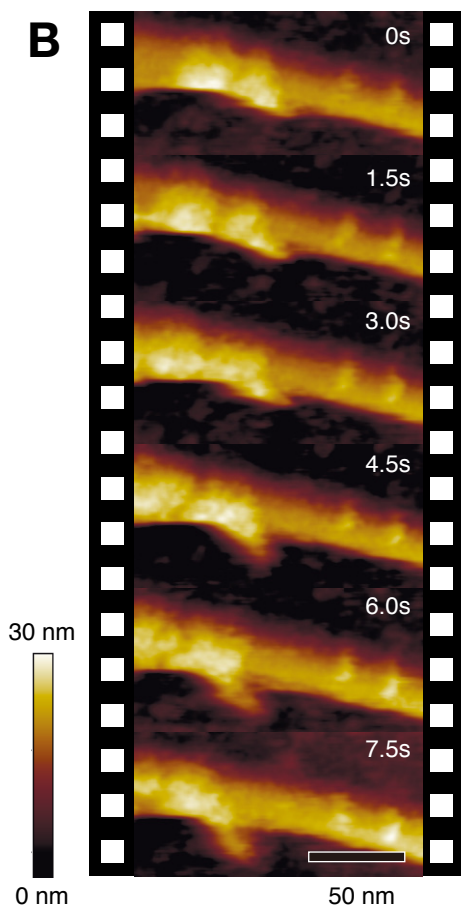
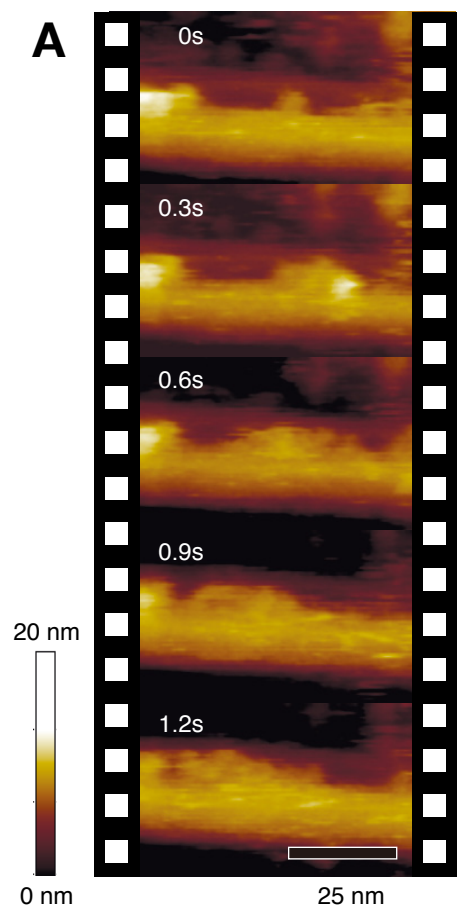


Fig. 4

